In situ x-ray scattering study on the evolution of Ge island morphology and relaxation for low growth rate: Advanced transition to superdomes

M.-I. Richard,[1,2] T. U. Schülli,[1] G. Renaud,[1] E. Wintersberger,[3] G. Chen,[3] G. Bauer,[3] and V. Holý[4]
[1]*Département de Recherche Fondamentale sur la Matière Condensée/SP2M/NRS, CEA Grenoble, 17 Avenue des Martyrs, F-38054 Grenoble Cedex 9, France*
[2]*ID01/ESRF, 6 rue Jules Horowitz, BP 220, F-38043 Grenoble Cedex, France*
[3]*Institut für Halbleiter- und Festkrperphysik, Johannes Kepler Universität Linz, 4040 Linz, Austria*
[4]*Faculty of Mathematics and Physics, Charles University, Ke Karlovu 5, 121 16 Prague, Czech Republic*
(Received 17 July 2008; revised manuscript received 17 June 2009; published 16 July 2009)

The kinetics of the growth of Ge superdomes and their facets on Si(001) surfaces are analyzed as a function of deposited Ge thickness for different growth temperatures and at a low growth rate by *in situ* grazing-incidence small-angle x-ray scattering in combination with *in situ* grazing-incidence x-ray diffraction. At a low growth rate, intermixing is found to be enhanced and superdomes are formed already at lower coverages than previously reported. In addition, we observe that at the dome-to-superdome transition, a large amount of material is transferred into dislocated islands, either by dome coalescence or by anomalous coarsening. Once dislocated islands are formed, island coalescence is a rare event and introduction of dislocations is preferred. The superdome growth is thus stabilized by the insertion of dislocations during growth.

DOI: 10.1103/PhysRevB.80.045313 PACS number(s): 61.05.C−, 81.07.Ta, 81.15.−z, 61.82.Fk

I. INTRODUCTION

The physical properties of semiconductor nanostructures depend entirely on their size, shape, and internal structure (strain and composition), which thus have to be fully controlled and understood. Semiconductor nanostructures are classically grown by the Stranski-Krastanow (SK) mechanism for which, beyond a critical thickness, islands are formed on a two-dimensional (2D) wetting layer. This is the case for the growth of Ge on Si(001) for which the 2D-three-dimensional (3D) transition is driven by the 4.16% lattice mismatch between Ge and Si, Ge having the larger lattice parameter. The mechanism of the SK growth of Ge layers on Si(001) substrates has been investigated extensively (see, e.g., Refs. 1 and 2 for a review). By increasing the Ge coverage above a critical thickness of ~4 monolayers (ML), islands that are coherent (i.e., without defects) appear. Square pyramids exposing {105} facets first form, followed by dome-shaped islands with {105}, {113}, and {15 3 23} facets, and a top (001) facet.[3] Another type of coherent islands called "barns" with additional {111} and {20 4 23} facets[4,5] may follow. For depositions higher than a threshold of about 9 ML,[5,6] the misfit strain can no longer be accommodated coherently and larger islands named "superdomes" with interfacial misfit dislocations appear. They expose similar facets as barns but with different relative sizes.

The coherent pyramid and dome-shaped islands have been the subject of many very detailed recent studies that deal with their growth[5,7,8] as well as with their strain and composition.[9–11] For instance, different concepts on the role of strain relaxation, diffusion and temperature activation have been reported to describe Ge-Si intermixing in Ge nanostructures on Si(001) (Ref. 1) and Si(111).[12,13] In contrast, much less work[14] has been done in characterizing the superdomes. The kinetics of the superdome growth and of their shape transitions is still not completely understood. In particular, the evolution with the *growth rate*, with *temperature*,[15] and *deposited thickness* of the superdome apparition, size, and shape were not fully determined during growth. For example, Eaglesham *et al.*[16] reported that islands grown at 773 K and with a height above 50 nm are no more dislocation-free. From x-ray reflectivity measurements[17] on islands grown at 823 K with a very low growth rate, the island-height evolution was determined as a function of Ge deposition, exhibiting a sudden increase in island height at ~6 ML coverage. Apparently, at the transition, a huge amount of material is transferred into dislocated islands, either by island coalescence or by anomalous coarsening.

In this work we report on extensive *in situ* investigations of Ge island growth. The morphology of islands during their growth has been investigated so far by several *in situ* methods, such as electron or x-ray diffraction,[18] scanning tunneling, or low-energy electron microscopies.[8,19] Recently, grazing-incidence x-ray scattering (GISAXS) (Ref. 20) was used to analyze the shape and size of growing metallic islands. It has been shown to be a powerful tool in analyzing the faceting of semiconductor islands and in indexing their facets.[21] With *in situ* GISAXS, contrary to other *in situ* techniques, not only the average diameter and height of the islands but also the average size of each facet can be directly determined during growth. In addition, *in situ* GISAXS was combined with grazing-incidence x-ray diffraction (GIXD), which allows monitoring the island nucleation by the beginning of lattice relaxation and following the evolution of the strain state. We report here on a combined GISAXS-GIXD study performed *in situ*, during the growth of Ge on Si(001) at a low growth rate and at different temperatures. The transition from the wetting layer to the dome and superdome formations is detected and quantitatively characterized by both techniques.

II. EXPERIMENTS

The samples were grown by molecular-beam epitaxy (MBE) in a dedicated ultrahigh vacuum chamber equipped

 ©2009 The American Physical Society

with large beryllium windows and coupled to a surface diffractometer for GIXD and GISAXS measurements, on the BM32 synchrotron beamline at the ESRF, Grenoble.[22] The base pressure of the ultrahigh vacuum chamber is a few 10^{-11} mbar. The Si(001) substrates were deoxidized by annealing at 1200 K until a sharp 2×1 reconstructed reflection high-energy electron diffraction (RHEED) pattern was observed. Germanium was deposited with a Knudsen cell with a slow deposition rate of 170 s for one Ge ML ($\sim$0.006 ML/s), which was *in situ* calibrated using both a quartz microbalance and x-ray reflectivity. This rate is about seven times smaller than the deposition rate usually used for Ge/Si MBE experiments.[7] Ge was deposited monolayer after monolayer at four growth temperatures (773, 823, 873, and 923 K). After growth, no damage induced by x rays was observed. We have experimentally determined with GISAXS and GIXD that no evolution of the island morphology, internal structure, or composition happens during annealing below 773 K. At 823 K, small changes were found to start only after 30 s of annealing, which confirms the observation of Medeiros-Ribeiro *et al.*[23] To avoid any evolution of the islands between successive depositions, the samples were immediately cooled down to 723 K after each added monolayer, the reference temperature at which the x-ray measurements were performed. These typically lasted 50 min, after which the temperature was raised again to the deposition temperature. During cooling or heating, the sample never stayed more than 30 s at intermediate temperatures between 773 K and the growth temperature so that significant morphological evolution or Si-Ge intermixing between successive depositions can be safely neglected.[8,21,23] We actually checked that, for a growth temperature of 923 K, almost the same final state (as probed with GISAXS and GIXD) was obtained for a 7 ML deposition realized with the procedure described above, and a 7 ML deposition without growth interruption. Consequently, our successive depositions are equivalent to a continuous deposition with constant rate as a function of time; the deposited amount θ (Ge coverage) is proportional to an equivalent deposition time t.

For all x-ray measurements, the x-ray beam energy was set at 11 043 eV and the incident angle fixed at the critical angle for total external reflection of Si, $\alpha_i=0.163°$. The incident beam of 1 mrad (horizontal—H) $\times$0.1 mrad (vertical—V) divergence, was defined by a pair of slits to 0.1 mm(H)$\times$0.3 mm(V) at the sample position, the horizontal direction being perpendicular to the surface.

For GIXD measurements, the scattered beam direction was defined by a slit opening of 1 mm parallel to the surface and an 8 mm slit perpendicular to it. The slit-to-sample distances were 200 and 600 mm, respectively. For GISAXS measurements, slits and a beam stop were used in vacuum to avoid background scattering by the beryllium windows. The scattered intensity was detected by a two-dimensional low-noise charge-coupled device detector from Princeton (1152 $\times$1242 pixels of 56.25×56.25 μm^2) placed 1.68 m away from the sample. All direct- or reciprocal-space notations refer to the bulk Si unit cell ($a=b=c=5.431$ Å and $\alpha=\beta=\gamma=90°$). The Miller indexes (h, k, and l) are expressed in reciprocal-lattice units of Si.

GIXD measurements were performed mostly along the ($h0l$) direction (h being variable and l being small: $l=0.04$), with finer measurements in the vicinity of the Si(400) and Ge(400) Bragg peaks (Fig. 1). These radial scans were recorded *in situ* for each added monolayer. GISAXS measurements consisted in recording two-dimensional GISAXS intensity distributions with the x-ray beam aligned along the substrate's [100], [110], (Fig. 2) and [15 3 0] (Fig. 3) directions. The GISAXS maps represent cuts of the three-dimensional intensity distribution in reciprocal space with

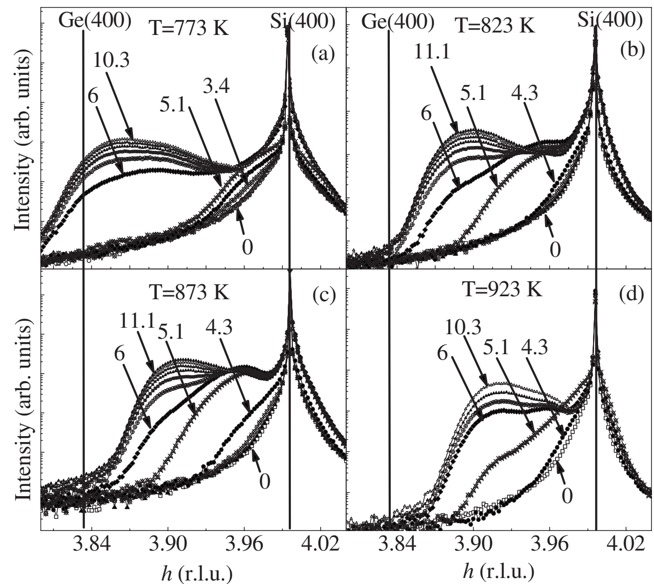

FIG. 1. GIXD data: radial scans along the $\langle h0l\rangle$ direction, with $l=0.04$, in the vicinity of the Si(400) reflection, for different Ge depositions indicated in the graphs in equivalent monolayers (ML). The vertical lines show the position of the bulk Si(400) and Ge(400) Bragg peaks. The growth temperatures are(a) 773 K (from 0 to 10.3 ML), (b) 823 K (from 0 to 11.1 ML), (c) 873 K (from 0 to 10.3 ML), and (d) 923 K (from 0 to 11.1 ML).

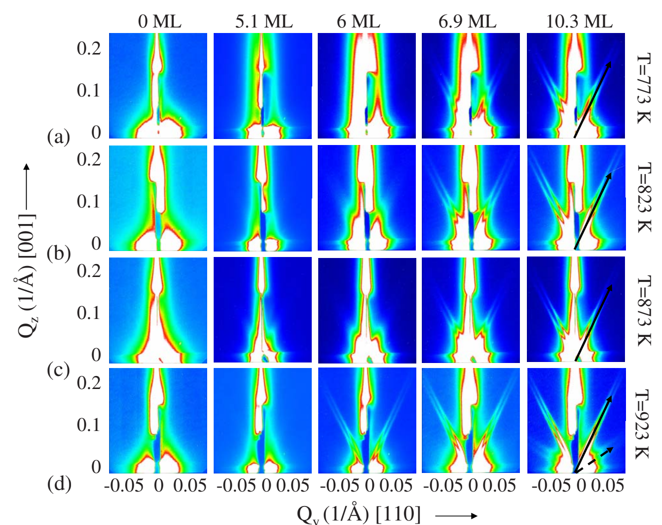

FIG. 2. (Color online) GISAXS intensity maps along the [110] azimuth obtained at growth temperatures of (a) 773, (b) 823, (c) 873, and (d) 923 K; the numbers denote the number of deposited Ge monolayers, the arrows are along $\langle 113\rangle$ (full arrows) and $\langle 111\rangle$ (dashed arrow).

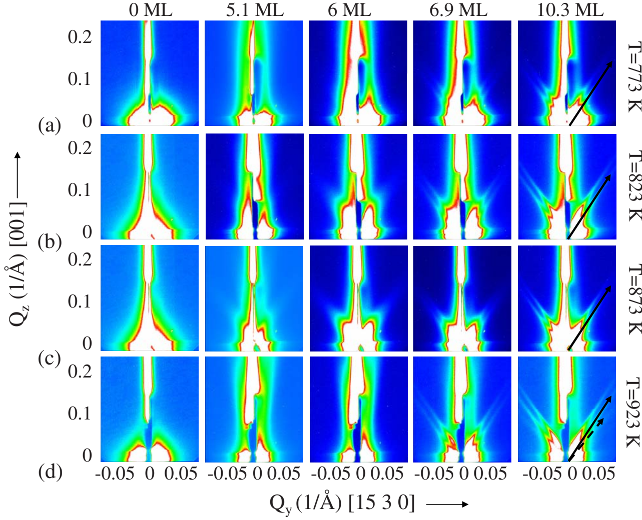

FIG. 3. (Color online) GISAXS intensity maps along the [15 3 0] azimuth obtained at growth temperatures of (a) 773, (b) 823, (c) 873, and (d) 923 K; the numbers denote the number of deposited Ge monolayers, the arrows are along ⟨15 3 23⟩ (full arrows) and ⟨20 4 23⟩ (dashed arrow).

the Ewald sphere. The scattering vector is defined as $\mathbf{Q}=\mathbf{K}_f-\mathbf{K}_i$ ($\mathbf{K}_{i,f}$ are the wave vectors of the primary and scattered beams, respectively, having the angles $\alpha_{i,f}$ with the mean sample surface). The collected images correspond to (Q_yQ_z) planes, which are tangential to the Ewald sphere.

III. GISAXS ANALYSIS

For the analysis of the GISAXS data we have used the distorted-wave Born approximation.[24] From this approach it follows that the intensity scattered by a noncapped island is a coherent superposition of four scattering processes. If we assume that the island positions are completely random and that the islands are far apart from each other, the intensity of the scattered radiation is an incoherent superposition of intensities scattered by individual islands

$$I(\mathbf{Q}) = \text{const}\sum_{n=1}^{4}\sum_{m=1}^{4} A_n A_m^* \langle \Omega^{\text{FT}}(\mathbf{Q}_n)\Omega^{\text{FT}*}(\mathbf{Q}_m)\rangle, \quad (1)$$

where the sums run over the scattering processes, and A_n and $\mathbf{Q}_n$ are the amplitude and scattering vector of process n. The direct (kinematical) process $n=1$ is the scattering of the incident wave while the indirect processes $n=2,3,4$ imply reflections on the substrate and correspond to the multiple-scattering paths displayed in Fig. 4—see Ref. 24 for details. $\Omega^{\text{FT}}(\mathbf{Q})$ is the Fourier transform of the shape function $\Omega(\mathbf{r})$ of a single island and the averaging in Eq. (1) is carried out over all island sizes.

In the case of islands with flat facets, it is suitable to convert the volume integral calculating $\Omega^{\text{FT}}(\mathbf{Q})$ into an integral over the island surface $S(\Omega)=\cup_j S^{(j)}$ using the Stokes formula, which yields

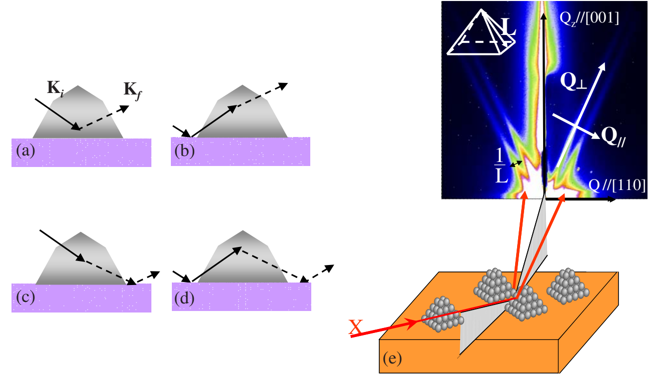

FIG. 4. (Color online) [(a)–(d)] Four scattering processes in GISAXS. $\mathbf{K}_{i,f}$ are the wave vectors of the primary and scattered beams, respectively. (e) Schematic drawing of islands and their corresponding GISAXS intensity map. The width of the streak is inversely proportional to the facet size L.

$$\Omega^{\text{FT}}(\mathbf{Q}) = \frac{i}{Q^2}\sum_j Q_\perp^{(j)} e^{-iQ_\perp^{(j)} r_\perp^{(j)}} F_j(\mathbf{Q}_\parallel^{(j)}). \quad (2)$$

In this equation, if we denote by $\mathbf{n}^{(j)}$ the unit vector of the outer normal of the facet j with the area $S^{(j)}$, then $r_\perp^{(j)}=\mathbf{r}.\mathbf{n}^{(j)}$ is the distance of this facet from the origin (located at the center of the bottom of the islands), $Q_\perp^{(j)}=\mathbf{Q}.\mathbf{n}^{(j)}$ is the component of $\mathbf{Q}$ perpendicular to the facet, and $\mathbf{Q}_\parallel^{(j)}=\mathbf{n}^{(j)}\times(\mathbf{Q}\times\mathbf{n}^{(j)})$ is the component of $\mathbf{Q}$ parallel to the facet. We have also denoted $F_j(\mathbf{Q}_\parallel^{(j)})=\int_{S^{(j)}} d^2\mathbf{r}_\parallel^{(j)} e^{-i\mathbf{Q}_\parallel^{(j)}.\mathbf{r}_\parallel^{(j)}}$ as the Fourier transformation of the shape function of the facet j.

Equation (2) makes it possible to analyze the contribution of individual facets to the intensity $I(\mathbf{Q})$. If we neglect tiny interference fringes (that are smeared out by the size averaging anyway), we can simplify the expression for the scattered intensity as follows:

$$I(\mathbf{Q}) \approx \text{const}\sum_j\sum_{n=1}^{4}|A_n|^2\left(\frac{Q_{\perp n}^{(j)}}{Q_n^2}\right)^2\langle|F_j(\mathbf{Q}_{\parallel n}^{(j)})|^2\rangle. \quad (3)$$

Within this approximation, the intensity is a sum of the contributions of individual facets. Each facet gives rise to a narrow streak in reciprocal space parallel to $\mathbf{n}^{(j)}$. The intensity distribution across the streaks is determined by $\langle|F(\mathbf{Q}_\parallel)|^2\rangle$, where the average is taken over by the distribution of facet sizes. A detailed numerical calculation of the shapes of the diffraction peaks from a set of facets with various shapes was performed using fast Fourier transform. It showed that the peak tails behave as $Q_\parallel^{-3}$, independently on the dispersion of the facet sizes. The full width at half maximum (FWHM) $\Delta Q_\parallel$ of the streak is inversely proportional to the mean facet size $L_0\equiv\langle L\rangle$ (Fig. 4); however, the proportionality factor decreases with increasing root mean square (rms) deviation σ_L of L. For $\sigma_L\to 0$, $L_0\to 2\pi/\Delta Q_\parallel$ holds. Along the streak, the intensity drops as $(Q_\perp^{(j)})^{-2}$. In the case of a nonfaceted island with a rounded surface, the scattered intensity decreases as Q^{-4} (the Debye-Porod law[25]) so that from the asymptotic intensity decrease it is possible to identify individual facets.

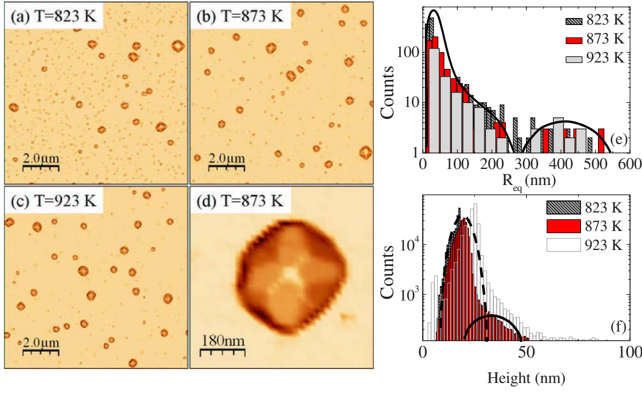

FIG. 5. (Color online) (a) AFM images of samples obtained after the deposition of 10–11 ML of Ge at (a) 823, (b) 873, and (c) 923 K, on a large scale, showing the presence of two island "families" with different mean sizes. (d) AFM zoom of a superdome island grown at 873 K. The measured mean sizes of {113} and {15 3 23} facets are ~145 and ~92 nm, respectively. They correspond to the simulated values observed in Figs. 8(a) and 8(b). (e) AFM histogram of the equivalent radii of the islands obtained from the island-projected area and (f) AFM histogram of the island heights as a function of the growth temperatures.

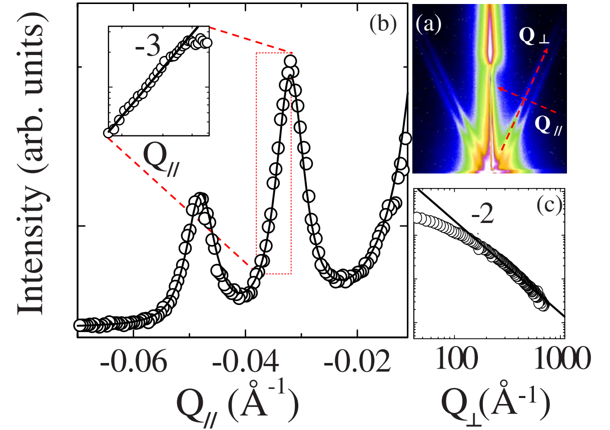

FIG. 6. (Color online) (a) GISAXS image (azimuth [110], $\theta = 10$ ML), from which the line scans in panels (b) and (c) are extracted along the $Q_\parallel$ and $Q_\perp$ axes. (b) The linear scan extracted from the GISAXS intensity map across the {113} facet streak (points) and its fit by a sum of three $f(Q_\parallel)$ functions (see text); the inset shows the tail of this line scan in a log-log representation. (c) Line scan along the facet streak. From (b) and (c), the $Q_\perp^{-2}$ and $Q_\parallel^{-3}$ slopes are visible.

The indirect scattering processes ($n=2,3,4$) give rise to an additional streak for each facet if $Q_{nz}>0$. Due to the reflection from the free surface, the additional streak is shifted vertically by $2K \sin \alpha_i$ and its intensity depends on the incidence or exit angles due to the reflectivity coefficients $r_{i,f}$. This effect has to be taken into account in the determination of the facet size from the streak width. The influence of the indirect scattering processes is visible in the experimental data taken along the [110] and [15 3 0] azimuths in Fig. 2 and 3, where the streaks are twofold.

Atomic force microscopy (AFM) measurements were performed *ex situ* on the samples after growth, i.e., for conditions corresponding to the total amount of deposited Ge. The AFM pictures of the surfaces [Figs. 5(a)–5(d)], and the histograms of the equivalent disk radius and heights of the islands [Figs. 5(e) and 5(f)] revealed that the island-size distribution is bimodal; small islands coexist with islands having a width and a height larger than 400 and 25 nm, respectively. Due to their larger scattering volume, the large ones dominate the GISAXS. Taking only into account the population of large islands, the rms deviation of the island sizes, $\sigma_L/L_0=0.17\pm0.03$, was obtained from the analysis of the AFM images.

In order to determine the evolution of the facet sizes, we have extracted line scans perpendicular to the streaks from the measured intensity maps and we have fitted the streak profile by a pair of modified Lorentzian functions $f(Q_\parallel) = \text{const}[1+(2Q_\parallel/\Delta Q_\parallel)^2(2^{2/3}-1)]^{-3/2}$ ($\Delta Q_\parallel$ is the FWHM of the function), obeying the asymptotic decrease ($|\mathbf{Q}_\parallel|^{-3}$) of the scattered intensity and yielding perfect fits. From direct numerical simulations it follows that, for this value of σ_L, the FWHM of the streak is $\Delta Q_\parallel \approx 2\pi/L_0$ with the accuracy of about 10%. The distance between the peaks stemming from various scattering processes is $\delta Q_\parallel = 2K \sin \alpha_i \sin \beta$, where β is the angle of the facet with the surface normal (001).

Figure 6 shows an example of a fit of a line scan extracted from the GISAXS measurement in the [110] azimuth for a deposition of 10 ML of Ge for the growth temperature of 873 K. This line scan is fitted by the sum of three modified Lorentzian functions, one corresponds to the streak of the top facet (001) (on the right side of the figure) while the other two stem from {113} facets. The study was not performed for the {105} facets appearing in the [100] azimuth because the flat-facet orientation (11° with respect to the [001] axis) and the small facet size induce a broadening of the {105} diffuse streaks that makes the extraction difficult. Therefore, only the {113} and {15 3 23} facet sizes were characterized. The insets in Fig. 6 show the linear scans extracted from the intensity map in the [110] azimuth for $\theta=10$ ML at a growth temperature of 873 K along and across the intensity streaks. The above predicted $Q_\parallel^{-3}$ asymptotic dependence is clearly visible. The values of the mean sizes L_0 for the islands corresponding to the total amount of deposited Ge deduced from these fits are consistent with those deduced from the *ex situ* AFM measurements performed after growth (Fig. 5).

IV. EXPERIMENTAL RESULTS AND ANALYSIS

GIXD (Fig. 1) and GISAXS (Figs. 2 and 3) measurements were combined to have access to composition and strain (GIXD) as well as also to the morphology (GISAXS) of the growing islands. Figure 1 shows the GIXD measurements performed around the Si(400) Bragg peak at 773, 823, 873, and 923 K. Figures 2 and 3 show the corresponding GISAXS maps as a function of the Q_y and Q_z coordinates of the scattering vector, i.e., parallel and perpendicular to the sample surface, respectively, for the [110] (Fig. 2) and [15 3 0] (Fig. 3) azimuthal directions of the primary beam. The maps measured along the [100] azimuth are not shown because the expected scattering from {105} facets is hardly visible, being too close to the specular rod.

Below 2.6–3.4 ML (depending on the growth temperature) both GIXD and GISAXS measurements remain un-

changed. This is because of the growth of a perfectly strained (pseudomorphic) flat two-dimensional wetting layer, which scatters at the same location as the Si substrate. For depositions of 3–4 ML of Ge, depending on temperature, diffuse scattering appears in GIXD radial scans below the Si(400) Bragg peak, as well as faint changes in the GISAXS maps. These changes are in the form of diffuse intensity streaks (which are doubled as a consequence of the indirect scattering processes—see Sec. III) along ⟨113⟩ directions for the maps measured in the [110] azimuth (Fig. 2) and along ⟨15 3 23⟩ directions (Fig. 3) for the maps measured in the [15 3 0] azimuth. These streaks are signatures of the 2D-3D transition, with the formation of 3D islands on top of the wetting layer. These results show that GIXD is very sensitive to the onset of island nucleation by detecting the very first stages of relaxation of the island lattice.

Interpreting our results for GIXD and GISAXS, we can state that for $T=773$ K, the partially relaxed island volume does not increase rapidly until a coverage of about 5.1 ML is reached (Fig. 2). At this stage, no dome facets ({113} and {15 3 23}) are detected on the GISAXS images. {105} facets were detected but their streaks are too broad to be analyzed. Pyramid islands have thus been formed. These small islands are almost fully strained by the substrate: they have an in-plane lattice parameter very close to the Si one and the measured diffuse scattering mostly arises because of their small size. The scattered intensity is modulated by the form factor of pyramids.

At 6 ML, a huge increase in the diffuse scattering is observed on the GIXD scan [see Fig. 1(a)] and the diffuse signal moves toward much smaller h values. The signal can be attributed to much more relaxed islands. Indeed, due to the larger lattice parameter of Ge, the partially relaxed component due to germanium shifts to lower values of h and adopts a position close to that of bulk germanium. This coincides with the appearance of weak rods on the GISAXS pictures, corresponding to scattering by {113} and {15 3 23} facets, which are known to be present on Ge domes, barns, or superdomes on Si(001). The large lattice parameter of these islands, close to the value for bulk Ge, can only be explained by large plastically relaxed islands because coherent islands such as domes or barns are much more strained by the Si substrate.[26]

To demonstrate this, we performed finite element method (FEM) simulations, using a program developed by Priester and co-workers.[27] Assuming a coherent, i.e., pseudomorphically strained dome-shaped island of the size of ∼100 nm (as measured by GISAXS) of *even* pure Ge, the in-plane strain component ϵ_{xx}, defined with respect to the Si substrate lattice, was calculated [see Fig. 7(a)], and the scattered intensity was simulated [see Fig. 7(b)]. The main part of the simulated scattering is located around $h=3.945$. Only a weak shoulder is found around $h=3.89$, at the position of the experimental scattering intensity maximum: the average relaxation of the simulated island is far from being centered at the position of the experimental data and is shifted toward the position of the Si bulk Bragg peak. This demonstrates that the experimentally observed relaxation cannot be achieved by coherent elastic relaxation.

These large relaxed islands can thus be identified as large plastically relaxed, i.e., dislocated superdomes, exposing side

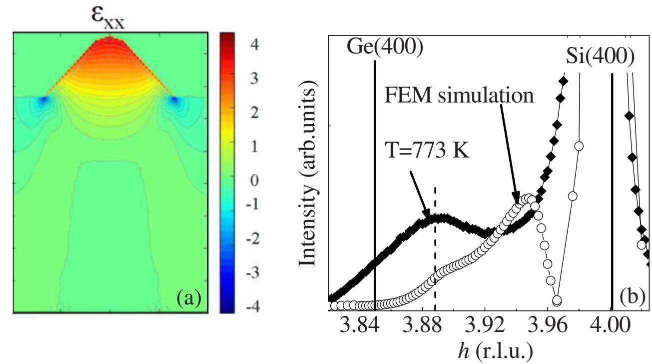

FIG. 7. (Color online) (a) FEM simulation of the in-plane deformation ϵ_{xx} in the island and the Si substrate underneath the island (with respect to Si bulk) in a 100-nm-large dome of pure Ge without dislocations. $\epsilon_{xx}=4.2\%$ means that Ge atoms are no more strained. In the region of the Si substrate, where $\epsilon_{xx}<0\%$, the Si lattice is compressed and where $\epsilon_{xx}>0\%$, the Si lattice is expanded. (b) Experimental and simulated scattered intensities. Finite element simulations of the strain state of coherent dome-shaped islands, and the corresponding simulation of the scattered intensity around the (400) reciprocal-lattice point show that their lattice parameter is much closer to that of Si than experimentally observed.

{113} and {15 3 23} facets. The GISAXS signal emanating from {111} facets of the superdomes is so small compared to the {113} ones that it is hardly detectable in the feet of the rods due to {113} facets. In contrast, the average relaxation at coverage of 5.1 ML in Figs. 1(b) and 1(c) could be achieved by coherent elastic relaxation, showing that, at this stage, coherent domes are formed. Thus, in the present study, superdomes appear for lower coverages than previously reported.[5,6] This can be explained by the much smaller deposition rate (0.0006 ML/s as opposed to 0.3 ML/s) in the present study. Rastelli *et al.*[6] observed the formation of superdomes after a deposition of 8 ML of Ge at 823 K at a rate of 0.3 ML/s. A slow growth rate leads to a more complete relaxation[17] by the introduction of dislocations, which can explain why dislocated islands are observed already at 6–6.9 ML for a growth temperature of 773 K in our case; this point will be discussed in next section in more detail. Note that very weak additional scattering streaks along ⟨111⟩ directions can be observed in the [110] azimuth for a deposition of 7–8 ML at 873 K and for a deposition of 10 ML at 823 K. At $T=923$ K, weak additional streaks along ⟨111⟩ appear in the [110] azimuth as early as 6 ML. The signal from the ⟨111⟩ streaks is clearly visible at 10 ML in Fig. 2(d). An onset of ⟨20 4 23⟩ streaks is also visible in Fig. 2(d), where its direction is denoted by a black arrow. The observation of the {111} and {20 4 23} facets in addition with AFM and the results of FEM simulations confirms the formation of dislocated superdomes after a deposit of 6 ML for the four studied temperatures. In GIXD scans, the pyramid- or dome-to-superdome transition is thus characterized by a strong strain relief causing a shift of the island-related maximum on the h axis to smaller h values.

In Fig. 8 we have plotted the dependence of the mean vertical sizes L_0 of the {113} and {15 3 23} facets for the growth temperatures of 773, 823, 873, and 923 K as a function of the deposited Ge coverage θ. Between 6 and 6.9 ML,

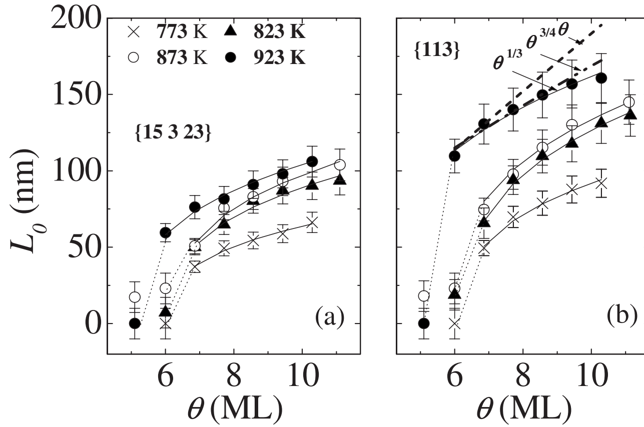

FIG. 8. The dependence of the mean facet sizes L_0 on the nominal coverage θ of the number of the deposited Ge monolayers is shown for the (a) {15 3 23} and (b) {113} facets, respectively. Above 6 ML at 923 K and 6.9 ML for the three other growth temperatures, the data were fitted to a $B(\theta-\theta_c)^{1/3}$ function (full lines).

a significant increase in the {113} and {15 3 23} facet sizes (Fig. 8) is observed. For instance, the mean size of the {113} facets increases from (0 ± 10) to (50 ± 5) nm between 6 and 6.9 ML deposits for the growth temperature of 773 K.

For $T=773$ K, above 6.9 ML, the facet size is found to evolve as $\theta^{1/3}$. This is shown in Fig. 8(b), where the dashed lines correspond to $\theta^{1/3}$, $\theta^{3/4}$, and θ^{1} power laws. This $\theta^{1/3}$ power law implies that, given certain assumptions, the island volume V is proportional to the deposited Ge coverage θ. The assumptions are that (i) the apparent shape anisotropy of the superdomes is neglected, and (ii) small volume variations possibly induced by a different size variation in the {105}, {111}, or {20 4 23} facet areas are also neglected. The first hypothesis, which postulates that the apparent anisotropy of the superdomes does not influence the analysis of the GISAXS data with respect to the 1/3 power law, is justified as GISAXS measurements average over the facet sizes. During the superdome evolution, the island shape is changed, which causes changes in the relative sizes of different facet types; however, the area limited by the {105} facets is negligible with respect to that limited by the other dome or superdome facets[5,6] so that the assumption (ii) is approximately valid as well. Furthermore, AFM images show that the area limited by the steep superdome facets ({111} and {20 4 23}) is almost negligible compared to the {113} and {15 3 23} superdome facets.

The 1/3 power-law observation excludes the possibility of the Ostwald ripening for which, according to Lifshitz-Slyozov,[28] Wagner,[29] and Chakraverty,[30,31] the island size should increase as $t^{3/4}$ or t^{1}, where t is the deposition time. Our results suggest that island coalescence occurs at the transition and, once dislocated islands are formed, the coalescence of islands is a rather rare event.[32,33] This is consistent with AFM images, which reveal a large separation of superdome islands. Besides, no depletion region is evident around the dislocated islands. This was previously observed by Merdzhanova *et al.*[14] for a faster growth rate (0.04 ML/s) and for a growth temperature around 843 K, and interpreted as the signature of a comparatively small efficiency of anomalous coarsening at low temperatures. Note that the 1/3 power evolution of superdome facet sizes is valid supposing that the number of superdomes remains constant with increasing Ge deposition, after the coherent-to-incoherent growth transition, whereas their size increases accordingly. Moreover, the total volume of the domes remain constant after this transition; this is confirmed by the GIXD data since, in Figs. 1(b) and 1(c), the signal from the domes, located in between the signal from superdomes and the Si Bragg peak, does not change beyond the deposition of 7 ML. As no decrease or increase in the intensity of the scattering from domes is observed, dome coalescence is a rare event and in average, domes do not increase in size. This implies that, when superdomes are formed, the deposited Ge atoms preferentially attach to superdomes and their mean facet sizes will follow a 1/3 power law. Nevertheless, island capture induced by diffusion-mediated processes[34–36] or anomalous coarsening[8,14] cannot be excluded as it corresponds to a small amount of captured material compared to the volume of superdomes.

During the superdome growth, the GIXD data show that the maximum of relaxation stays almost constant but that the corresponding intensity increases [see Fig. 1(a), between 6 and 10.3 ML]. This is interpreted as being caused by the growth of superdomes as confirmed by the increase in the {113} and {15 3 23} facet sizes found by GISAXS. In the following, we define ϵ^{Ge} as the residual strain of a Ge island (with respect to the relaxed Ge lattice) and $\epsilon_0=4.16\%$ as the mismatch between bulk Ge and Si. In a one-dimensional model of an island of width w, relaxed by n dislocations of Burgers vector b, one has $\epsilon^{\mathrm{Ge}}=\epsilon_0\text{-}nb/w$ (Ref. 37). The above results show that ϵ^{Ge} is constant above $\theta=6$ ML while w increases with $\theta^{1/3}$. Thus, n also increases with θ. This implies that during the superdome growth, the introduction of dislocations is prevalent compared to the coalescence of islands and it reduces the need for strain energy relief by elastic deformation.

The same phenomena are observed for the other studied growth temperatures. The strong strain relief and the shift of the island relaxation toward the position of the Ge bulk Bragg peak in GIXD can be correlated with the introduction of dislocations inside the islands and to the formation of superdomes. If we consider the growth temperature of 923 K, at the dome-to-superdome transition (between 5.1 and 6 ML), the mean size of the {113} and {15 3 23} facets increases from (0 ± 10) nm to (110 ± 11) nm and to (60 ± 6) nm, respectively, whereas the mean {113} facet size is around 30 nm for a domelike island according to Ref. 38. The transition from domes to superdomes does not only explain the significant increase in the facet sizes; a large amount of material is transferred into dislocated islands at the transition as seen by the huge increase in the scattered intensity in GIXD.

The superdome growth is thus characterized by two phenomena. First, at the transition, the coalescence of domes is the dominant pathway toward the formation of dislocated islands. Second, during the growth of superdomes, the fact that their volume growth is proportional to the deposit implies that superdome coalescence is a rare event. The introduction of dislocations prevails and the superdomes are char-

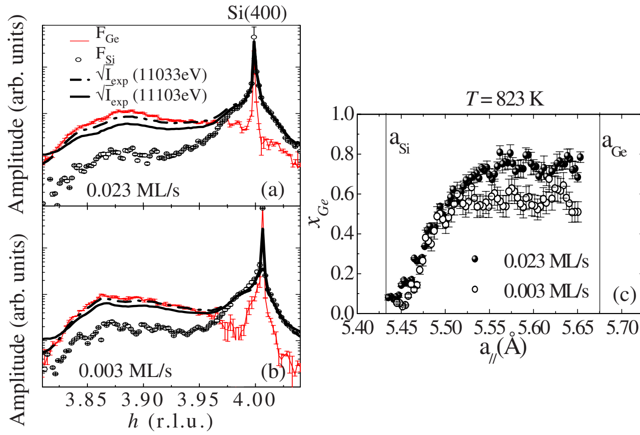

FIG. 9. (Color online) Experimental anomalous x-ray diffraction data ($\sqrt{I_{exp}}$) measured at two energies (11 033 and 11 103 eV), and Ge and Si structure factors (F_{Ge} and F_{Si}) calculated from the experimental anomalous x-ray diffraction data. The curves are plotted as a function of lattice parameter for a growth temperature of 873 K, a deposit of 8 ML, and for two growth rates: (a) 0.023 and (b) 0.003 ML/s. (c) Ge content of the islands determined from the ratio of the Ge and Si structure factors versus in-plane lattice constant.

acterized roughly by a self-similar volume increase. The {113} and {15 3 23} facets continue to grow and are not suppressed by the introduction of the steeper {111} and {20 4 23} facets.

From the fit of the experimentally determined mean facet sizes L_0 to the $\theta^{1/3}$ power law $L_0=B(\theta-\theta_c)^{1/3}$, where B and θ_c are constant, we determined the temperature dependence of the constant B for both investigated facet types. The value of $B_{\{113\}}/B_{\{15323\}}$ is found to be constant, around 1.5 ± 0.1 in the investigated temperature range, which implies that the superdome shape does not strongly depend on temperature.

From GIXD data taken after completing the deposition of Ge (10–11 ML), the average lateral lattice parameter of the superdomes was obtained as a function of temperature: 5.62 Å at 773 K, 5.58 Å at 823 K, 5.57 Å at 873 K, and 5.55 Å at 923 K. With increasing temperature, the average lattice parameter of the islands decreases. According to the findings in Ref. 14, this dependence is caused by the increase in the Si content for increasing growth temperature (see also Refs. 39–41). This has been confirmed by multiwavelength anomalous diffraction measurements performed at the end of each growth. As superdomes are formed at 6 ML at $T=923$ K and 6–6.9 ML at $T=773$ K, it appears that for a low growth rate the nucleation of dislocations is almost temperature independent. To determine if intermixing increases with growth rate, we performed multiwavelength anomalous x-ray diffraction measurements for two different growth rates (0.023 and 0.003 ML/s) at a growth temperature of 823 K for a deposit of 8 ML of Ge. In this experiment, we have compared the GIXD intensities measured for various photon energies around the Ge K edge, in various positions h in reciprocal space,[21] and we have extracted the Si and Ge structure factors (F_{Ge} and F_{Si}) as illustrated in Figs. 9(a) and 9(b). From the ratio of the Si and Ge structure factors, we determined the Ge content x_{Ge} of the islands as a function of in-plane lattice parameter [Fig. 9(c)]. From the figure it follows that the maximum Ge content in the island volume decreases with decreasing growth rate. Since the superdome shapes grown by different growth rates are similar, we conclude that the *average* Ge content in the island decreases with decreasing growth rate. This is the evidence that Si intermixing is enhanced for lower growth rates.

V. DISCUSSION

In the following, we propose a model to explain these observations. For this purpose, we will use the phenomenological relation given in Ref. 14, which links the critical volume to incorporate a dislocation to the Ge content: $x_{Ge}=3.7V_c^{-1/6}$, where V_c is expressed in nm^3 [see Fig. 2(d) of Ref. 14]. This relation was proven theoretically to be appropriate by Marzegalli *et al.*[42] who computed this critical volume for the onset of plastic strain relaxation in SiGe islands on Si(001) for different Ge contents and realistic shapes by using a three-dimensional model, with position-dependent dislocation energy. The average island volume expressed in nm^3 depends on the island density ρ (islands/nm^2), Ge coverage θ (atoms/nm^2), and island lattice parameter a (nm) as $V=\frac{a^3}{8}\frac{\theta}{\rho}$. The critical coverage, θ_c expressed in atoms/nm^2 at the dome-to-superdome transition is thus given by

$$\theta_c = \frac{8\rho V_c}{a^3} = \frac{8\times 3.7^6\rho}{x_{Ge}^6 a^3}, \tag{4}$$

where ρ, a, and V_c are expressed in islands/nm^2, nm, and nm^3, respectively. The Ge concentration x_{Ge} and the island density ρ can be written as a function of flux F at a given temperature. From Ref. 43, it can be shown that the average Ge fraction x_{Ge} decreases almost linearly with decreasing growth rate, F at 923 K: $x_{Ge}=x_1+x_2F$, x_1, and x_2 (min/ML) are some positive constants, with F expressed in ML/min. A decrease in the x_{Ge} value with decreasing F follows from our anomalous diffraction experiment (see Fig. 9).

From Ref. 44 (see Fig. 2) at 873 K, the island density increases with increasing F; $\rho=\beta F^{2/3}$, where β is a constant, ρ and F are expressed in islands/nm^2 and ML/min, respectively. Thus the critical coverage (expressed in atoms/nm^2) of the dome-to-superdome transition as a function of flux F at growth temperatures in the 873–923 K range is given by the following empirical relation:

$$\theta_c = \frac{8\times 3.7^6\beta F^{2/3}}{a^3(x_1+x_2F)^6}. \tag{5}$$

For small fluxes F, θ_c is growing while for fluxes above $\frac{x_1}{8x_2}$, it is decreasing [see Fig. 10(b)]. If we estimate $x_1=0.5$ and $x_2=0.006$ min/ML (Refs. 14 and 43) at 873–923 K, the critical coverage is an increasing function of the flux F for fluxes smaller than 0.174 ML/s. The flux of 0.006 ML/s [dashed line in Fig. 10(a)] used in this work is much smaller than the flux of 0.04 ML/s reported in Ref. 14 [full line in Fig. 10(a)], i.e., the one usually used in MBE growth of Ge islands. This explains our experimental results, namely, the advanced transition of domes to superdomes for the substantially lower Ge growth rate. From the rough estimation of the critical island volume for the dome-to-superdome transition, from the criti-

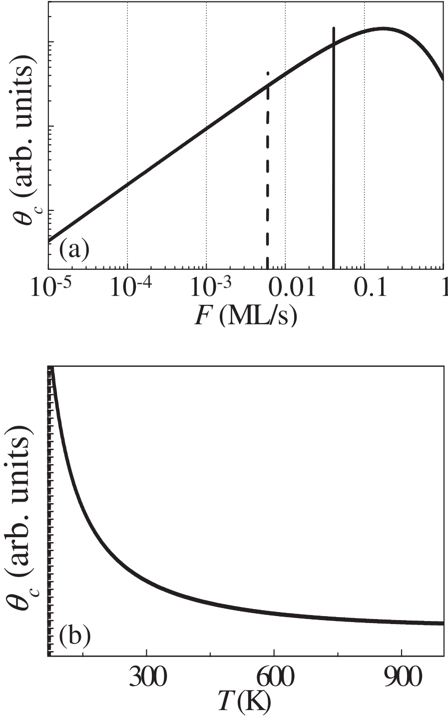

FIG. 10. Evolution of the critical coverage θ, for which dislocations appear, as a function of (a) flux F and (b) growth temperatures. The dashed and full lines in (a) indicate the growth rates used in this work and the one used in Ref. 14, respectively.

cal coverage θ_c, the critical Ge concentration $x_{\mathrm{Ge}}^{\mathrm{crit}} \approx 0.6$, and from the island density, we roughly estimated that the amount of Ge transferred from the wetting layer to the island is negligible at this transition. This finding is confirmed by experimental results published earlier,[21] showing that approximatively 1 ML of Ge is transferred from the wetting layer to the dome volumes. However, above the dome-to-superdome transition, the superdome volumes were found to grow linearly with the coverage, i.e., no Ge transfer from the wetting layer to the superdome volume was detectable.

The Ge content of the islands x_{Ge} and the island density ρ can also be written as a function of temperature at a given flux. With increasing temperature T, x_{Ge} decreases due to intermixing[41,45] and ρ decreases as well, fulfilling the Arrhenius law.[46] From Refs. 41 and 45, a phenomenological relation can be obtained for x_{Ge}: $x_{\mathrm{Ge}} \sim -0.1746 + 6.15 \times 10^8 T^{-3}$ (T is expressed in K) in the 0.035–0.33 ML/s range. In the following, we suppose that, at our growth rate (0.006 ML/s), this tendency is still applicable. From the AFM measurements of the studied samples, the evolution of the island density as a function of time has been determined as $\rho \sim 0.24 \times 10^{-9} e^{\delta/T}$ islands/nm^2, with $\delta \sim 7380$ K and T is the temperature. The critical coverage of the dome-to-superdome transition at a flux of 0.006 ML/s and as a function of temperature is then given by the following phenomenological relation:

$$\theta_c \sim \frac{8 \times 3.7^6 \times 0.24 \times 10^{-9} e^{\delta/T}}{a^3[-0.1746 + 6.15 \times 10^8 T^{-3}]^6}. \quad (6)$$

For T higher than 205 K, the critical coverage is decreasing as a function of growth temperature [see Fig. 10(b)]. At 973 K, dislocations will appear at a coverage that is only about ~ 0.25 ML smaller compared to one for which superdomes appear at a growth temperture of 723 K: $|\theta_c(T=923\ \mathrm{K}) - \theta_c(T=723\ \mathrm{K})| \sim 1.54$ atoms/nm$^2 \sim 0.25$ ML, assuming that the islands consist of pure Ge. Thus for our work follows that the critical coverage is almost temperature independent, as experimentally observed.

VI. CONCLUSION

We have studied the evolution of the size of superdome facets of Ge islands on (001) Si substrates and their relaxation state for comparatively low growth rates, using *in situ* grazing-incidence small-angle x-ray scattering and diffraction. From the evolution of the widths of GISAXS intensity streaks in reciprocal space, we have determined the growth kinetics of the superdome {113} and {15 3 23} facets. The 1/3 power-law dependence of the superdome facet size on the amount of deposited Ge indicates that once dislocated islands are formed, the coalescence of islands, if any, is a rare event. However, Ostwald ripening and anomalous coarsening cannot be excluded. At the dome-to-superdome transition, a huge amount of material is transferred into dislocated islands either by dome coalescence or anomalous coarsening. From *in situ* grazing-incidence diffraction experiment it follows that the mean lateral lattice parameter of the superdomes remains constant during their growth. Thus, superdomes are stabilized by the insertion of dislocations during their growth. We also demonstrate that a low growth rate shifts the onset for dislocation formation to lower Ge coverages than for higher growth rates.

The strength of the present work lies in the direct determination, *in situ*, of the evolution of the statistical average of the facet sizes as a function of deposited material during the MBE growth under UHV conditions.

We show that *in situ* UHV-GISAXS measurements during MBE growth complement microscopic techniques and allows for a systematic study of the statistical average of facet sizes as a function of the deposited amount of Ge and of growth temperatures. Combined with *in situ* GIXD, it leads to a complete understanding of both strain status and composition as well as of the morphology of the islands.

We expect that the island evolution reported here can be employed for the study of other Stranski-Krastanow islands systems. A further step will consist in the characterization of defect formation and their evolution during the *in situ* growth of superdomes using quasiforbidden x-ray diffraction.[47,48]

ACKNOWLEDGMENTS

The authors thank C. Priester and V. Favre-Nicolin for the development of the FEM and diffraction simulation programs. This work is a part of the research program MSM under Grant No. 0021620834 that is financed by the Ministry of Education of the Czech Republic. E.W., G.C., and G.B thank the FWF, Vienna, Austria (Project No. SFB025) for support. The authors acknowledge additional support from the EC network SANDiE.

[1] F. Ratto, G. Costantini, A. Rastelli, O. G. Schmidt, K. Kern, and F. Rosei, J. Exp. Nanosci. **1**, 279 (2006).
[2] J. Stangl, V. Holý, and G. Bauer, Rev. Mod. Phys. **76**, 725 (2004).
[3] G. Medeiros-Ribeiro, A. M. Bratkowski, T. I. Kamins, D. A. A. Ohlberg, and R. S. Williams, Science **279**, 353 (1998).
[4] E. Sutter, P. Sutter, and J. E. Bernard, Appl. Phys. Lett. **84**, 2100 (2004).
[5] M. Stoffel, A. Rastelli, J. Tersoff, T. Merdzhanova, and O. G. Schmidt, Phys. Rev. B **74**, 155326 (2006).
[6] A. Rastelli and H. Von Känel, Surf. Sci. Lett. **515**, L493 (2002).
[7] A. Rastelli, M. Stoffel, J. Tersoff, G. S. Kar, and O. G. Schmidt, Phys. Rev. Lett. **95**, 026103 (2005).
[8] F. M. Ross, R. M. Tromp, and M. C. Reuter, Science **286**, 3 (1999).
[9] G. Katsaros, G. Costantini, M. Stoffel, R. Esteban, A. M. Bittner, A. Rastelli, U. Denker, O. G. Schmidt, and K. Kern, Phys. Rev. B **72**, 195320 (2005).
[10] A. Malachias, S. Kycia, G. Medeiros-Ribeiro, R. Magalhães-Paniago, T. I. Kamins, and R. Stanley Williams, Phys. Rev. Lett. **91**, 176101 (2003).
[11] U. Denker, M. Stoffel, and O. G. Schmidt, Phys. Rev. Lett. **90**, 196102 (2003).
[12] F. Ratto, A. Locatelli, S. Fontana, S. Kharrazi, S. Ashtaputre, S. K. Kulkarni, S. Heun, and F. Rosei, Small **2**, 401 (2006).
[13] N. Motta, F. Boscherini, A. Sgarlata, A. Balzarotti, G. Capellini, F. Ratto, and F. Rosei, Phys. Rev. B **75**, 035337 (2007).
[14] T. Merdzhanova, S. Kiravittaya, A. Rastelli, M. Stoffel, U. Denker, and O. G. Schmidt, Phys. Rev. Lett. **96**, 226103 (2006).
[15] D. J. Eaglesham and R. Hull, Mater. Sci. Eng., B **30**, 197 (1995).
[16] D. J. Eaglesham and M. Cerullo, Phys. Rev. Lett. **64**, 1943 (1990).
[17] A. A. Williams, J. M. C. Thornton, J. E. Macdonald, R. G. van Silfhout, J. F. van der Veen, M. S. Finney, A. D. Johnson, and C. Norris, Phys. Rev. B **43**, 5001 (1991).
[18] M. Takahasi, T. Kaizu, and J. Mizuki, Appl. Phys. Lett. **88**, 101917 (2006).
[19] O. Kirfel, E. Müller, D. Grützmacher, K. Kern, A. Hesse, J. Stangl, V. Holý, and G. Bauer, Appl. Surf. Sci. **224**, 139 (2004).
[20] G. Renaud, R. Lazzari, Ch. Revenant, A. Barbier, M. Noblet, O. Ulrich, F. Leroy, J. Jupille, Y. Borensztein, C. R. Henry, J.-P. Deville, F. Scheurer, J. Mane-Mane, and O. Fruchart, Science **300**, 1416 (2003).
[21] T. U. Schülli, M.-I. Richard, G. Renaud, V. Favre-Nicolin, E. Wintersberger, and G. Bauer, Appl. Phys. Lett. **89**, 143114 (2006).
[22] http://www.esrf.eu/UsersAndScience/Experiments/CRG/BM32
[23] G. Medeiros-Ribeiro, T. I. Kamins, D. A. A. Ohlberg, and R. Stanley Williams, Phys. Rev. B **58**, 3533 (1998).
[24] M. Rauscher, R. Paniago, H. Metzger, Z. Kovats, J. Domke, J. Peisl, H.-D. Pfannes, J. Schulze, and I. Eisele, J. Appl. Phys. **86**, 6763 (1999).
[25] A. Guinier and G. Fournet, *Small Angle Scattering of X-rays* (Wiley, New York, 1955).
[26] M.-I. Richard, T. U. Schülli, C. Priester, V. Favre-Nicolin, and G. Renaud (unpublished).
[27] V. Ranjan, G. Allan, C. Priester, and C. Delerue, Phys. Rev. B **68**, 115305 (2003).
[28] I. M. Lifshitz and V. V. Slyozov, J. Phys. Chem. Solids **19**, 35 (1961).
[29] C. Wagner, Z. Elektrochem. **65**, 581 (1961).
[30] B. K. Chakraverty, J. Phys. Chem. Solids **28**, 2401 (1967).
[31] B. K. Chakraverty, J. Phys. Chem. Solids **28**, 2413 (1967).
[32] P. Meakin, Rep. Prog. Phys. **55**, 157 (1992).
[33] J. L. Viovy, D. Beysens, and C. M. Knobler, Phys. Rev. A **37**, 4965 (1988).
[34] P. A. Mulheran and J. A. Blackman, Phys. Rev. B **53**, 10261 (1996).
[35] F. Ratto, T. W. Johnston, S. Heun, and F. Rosei, Surf. Sci. **602**, 249 (2008).
[36] F. Ratto, A. Locatelli, S. Fontana, S. Kharrazi, S. Ashtaputre, S. K. Kulkarni, S. Heun, and F. Rosei, Phys. Rev. Lett. **96**, 096103 (2006).
[37] F. K. LeGoues, M. C. Reuter, J. Tersoff, M. Hammar, and R. M. Tromp, Phys. Rev. Lett. **73**, 300 (1994).
[38] A. Rastelli, M. Kummer, and H. von Kanel, Phys. Rev. Lett. **87**, 256101 (2001).
[39] D. J. Smith, D. Chandrasekhar, S. A. Chaperro, P. A. Crozier, J. Drucker, M. Floyd, M. R. McCartney, and Y. Zhang, J. Cryst. Growth **259**, 232 (2003).
[40] M. Floyd and Y. Zhang, Appl. Phys. Lett. **82**, 1473 (2003).
[41] T. U. Schülli, M. Stoffel, A. Hesse, J. Stangl, R. T. Lechner, E. Wintersberger, M. Sztucki, T. H. Metzger, O. G. Schmidt, and G. Bauer, Phys. Rev. B **71**, 035326 (2005).
[42] A. Marzegalli, V. A. Zinovyev, F. Montalenti, A. Rastelli, M. Stoffel, T. Merdzhanova, O. G. Schmidt, and L. Miglio, Phys. Rev. Lett. **99**, 235505 (2007).
[43] E. P. McDaniels, Q. Jiang, P. A. Crozier, J. Drucker, and D. J. Smith, Appl. Phys. Lett. **87**, 223101 (2005).
[44] B. Cho, T. Schwarz-Selinger, K. Ohmori, D. G. Cahill, and J. E. Greene, Phys. Rev. B **66**, 195407 (2002).
[45] G. Capellini, M. De Seta, and F. Evangelisti, Appl. Phys. Lett. **78**, 303 (2001).
[46] J. S. Sullivan, H. Evans, D. E. Savage, M. R. Wilson, and M. G. Lagally, J. Electron Mater. **28**, 426 (1999).
[47] M.-I. Richard, T. H. Metzger, V. Holý, and K. Nordlund, Phys. Rev. Lett. **99**, 225504 (2007).
[48] M.-I. Richard, A. Malachias, J.-L. Rouvière, T.-S. Yoon, Y.-H. Xie, V. Holý, E. Holmström, K. Nordlund, and T.-H. Metzger, (unpublished).